# Effects of Chain Length and Heat Treatment on the Nanotribology of Alkylsilane Monolayers Self-Assembled on a Rough Aluminum Surface

**Om P. Khatri,[†] Colin D. Bain,[‡] and Sanjay K. Biswas*,[†]**

*Department of Mechanical Engineering, Indian Institute of Science, Bangalore - 560012, India, and Department of Chemistry, University of Oxford, Mansfield Rd., Oxford OX1 3TA, United Kingdom*

*Received: July 23, 2005; In Final Form: September 21, 2005*

The conformational order of alkylsilane monolayers self-assembled on a rough aluminum surface is affected by the molecular chain length and the thermal history of the sample. These monolayers have been characterized by grazing angle FTIR spectroscopy. Tribological mechanisms were explored using initial molecular conformation order, sliding distance, normal load, and substrate compliance as experimental variables. Results indicate that the initial conformational disorder of the molecules determines the level of friction at the commencement of sliding. Adverse changes in dynamic friction and monolayer life during sliding are not thermally induced but are related to substrate roughness and local plasticity. Plastic deformation reduces the spatial density of the alkylsilane monolayer and is accentuated by an increase in the normal load.

## Introduction

In recent years, there has been much interest in the properties of organic ultrathin films deposited on solid surfaces such as gold, silver, aluminum, silicon, and mica. These thin films typically comprise a chemisorbed monolayer formed by spontaneous organization of long-chain molecules on the solid substrates.[1] Alkylsilane and alkanethiol molecules, particularly those with long alkyl chains, form well-ordered robust monolayers and are effective boundary lubricants,[2−8] reducing friction and improving wear resistance of the substrate.[4,5,9,10] Lubrication has been demonstrated even in situations where contact pressures and temperatures are high.[3,11,12] In this paper, we study the lubricating properties of alkylsilane monolayers on aluminum, a material that despite being a futuristic structural material has attracted scant attention from tribologists. Aluminum is a fascinating material to lubricate, as it is naturally covered with tenacious and thin oxide/hydroxide overlayers,[13] which provide good anchoring sites for alkylsilane additive molecules. Further, it is more easily deformed and more difficult to polish compared to other well-researched substrates such as steel and silicon. In real machinery, an additive dispersed in oil forms a monolayer at the tribological interface. The friction coefficient and the robustness of the monolayer control the power dissipation and life of the machine, especially if the operation takes the tribology into the boundary lubrication regime. We study here the friction and wear when alkylsilane monolayers assembled on a rough aluminum surface are slid against a steel ball. Avenues of energy dissipation, which may exist initially or which may be created during a tribological process, control friction and wear. The experiments are designed to elucidate dissipation mechanisms and their relationship with conformational order of the molecules in the monolayer, substrate roughness, and substrate plasticity.

The structure of alkylsilane monolayers, particularly octadecyltrichlorosilane (ODTS), on silicon, mica, and aluminum has been studied by vibrational spectroscopy,[14−17] contact angle measurement,[16,18−21] atomic force microscopy (AFM),[4,7,11,19−22] ellipsometry,[16,18,20,21] and X-ray photoelectron spectroscopy.[18,21] Recently, there has been much interest in correlating the structural organization of such self-assembled monolayers (SAMs) with frictional properties. There are a number of external parameters that may influence structural organization such as deposition time,[20] deposition temperature,[16,23] additives concentration,[24] presence of water,[25,26] and chain length.[14,27] A well-ordered alkylsilane monolayer in all-trans conformation is found only when the preparation temperature is below a critical value.[23] Conformational order and coverage increase with chain length.[16,20] Alkyltrichlorosilanes are susceptible to hydrolysis. It is generally believed that during SAM formation the Si−Cl group is hydrolyzed in the presence of interfacial water and/or hydroxyl groups on the substrate, to form silanol groups. Some of these groups bind to the substrate,[25,26] while others form cross-links to adjacent molecules by a condensation reaction, forming a dense chemically, mechanically, and thermally stable alkylsilane monolayer.[17,18,28]

In studying the friction of self-assembled monolayers in the surface force apparatus (SFA), Yoshizawa et al.[3] proposed that the friction coefficient is related to the crystallinity of the molecule; with a loss of crystallinity, the monolayer obtains the ability to rearrange and interdigitate across an interface, which increases friction. AFM studies on alkylsilane monolayers with different chain lengths[22] came to the conclusion that the high friction of conformationally disordered short-chain SAMs is due to an increase in the number of energy dissipation modes. There is a growing consensus that a decrease in crystallinity, molecular order,[14,27] and packing density[4,6] brought about by a reduction in chain length or any other means such as heating,[12] an increase in sliding velocity,[3,4,29] or a change in relative humidity[3,8] opens up more avenues of energy dissipation and hence enhances friction. Molecular dynamics simulations,[30,31] lateral force microscopy (LFM),[22,32,33] and nanotribological studies[34] have shown that the deformation of the monolayer by normal loading and shear increases disorder and therefore friction. It is implicitly assumed in the works quoted above that

* Corresponding author. Tel.: +91-80-2293 2512, 2351. Fax: +91-80-2360 0648. Email address: skbis@mecheng.iisc.ernet.in.
† Indian Institute of Science.
‡ University of Oxford.

10.1021/jp054074e CCC: $30.25 
Published on Web 11/17/2005

the more disorder there is initially in the monolayer, the less the ability of the monolayer to resist further disordering under load. Zhang and Archer[4] showed that the friction force increased more rapidly with increasing velocity when the packing density was lowered, and Salmeron et al.[7,22] showed explicitly in frictional force measurements that friction increases more rapidly with increasing normal load when the chain length is lowered.

The studies quoted above have been performed with the lateral force mode of the atomic force microscope. While the actual findings are of relevance to the design of micro- and nanomachines and magnetic storage devices, their relevance to problems in a wider domain and scale of tribology needs scrutiny. In nanotribology, a flat substrate carrying a SAM slides against a normally loaded spherical probe. While nanotribology allows, like AFM or LFM, the controlled probing of molecules anchored to a substrate in the form of a monolayer, in other respects such as contact pressures, contact scale (intermediate in order between AFM and macrotribology), and contact roughness (probe and substrate), the nanotribological configuration is unlike that achieved in a LFM experiment and approaches that of macrotribology.

Links between tribology at the molecular level and the macro level have intrigued practitioners and researchers for many years. Previous LFM and SFA studies of alkylsilane monolayers have been conducted on smooth and hard substrates; consequently, we have conducted nanotribological studies of this SAM on a silicon wafer both to compare the conclusions of LFM/SFA studies with those in the nanotribometer and to serve as a benchmark for the behavior of SAMs on the rough, plastic surface of aluminum.

Since earlier studies have put much emphasis on the conformational order of the SAM, we have used chain length and heat treatment (both of which influence the conformational order) as model variables to study friction and wear. It is well-known that the peak frequency and bandwidth of the methylene stretching modes is related to the degree of conformational disorder (gauche defects) in a long hydrocarbon chain.[35−38] Fourier transform (FT) IR studies of SAMs with different chain lengths show a decrease in conformational order with decreasing chain length.[14] When a self-assembled monolayer is heated, the molecules untilt, and the number of gauche defects increases, with the rate of disordering being related to the initial state of disorder at ambient temperature.[39] The effect of heat treatment on molecular disorder has been established for ODTS[17] and FOTS[40] (1H, 1H, 2H, 2H-perfluorooctyltrichlorosilane) SAMs on aluminum. We have shown that the monolayers become disordered with heating. For the FOTS monolayer, the initial level of order is recovered upon cooling back to room temperature from 423 K, but part of the disorder is retained if the monolayer is cooled back from higher temperatures. ODTS is less thermally stable and retains some disorder when cooled from 403 K. Here, we have prepared SAMs of alkylsilanes with three different lengths of their alkyl chains (8, 12, and 18) and heated them to different peak temperatures to obtain different levels of disorder before subjecting the SAMs to nanotribological tests.

In contrast to AFM or SFA studies, nanotribology provides access to information on the life of SAMs. Previous studies[32] have investigated the rigid-body motion of the molecules under tribological conditions, but we are still in the dark as to the relationship or relevance of the energy dissipation modes invoked to explain friction, to the life of these monolayers. Our present study is not conclusive on this point, but we are able to map the life of the molecule in terms of two variables, normal load and initial conformational order, which we demonstrate to have a strong influence on dissipation for the near-engineering configuration employed here.

## Experimental Section

**1. Materials and Sample Preparation.** Aluminum (Al is 97.25%, and the remaining 2.75% is Si, Mg, Mn, and Fe) and p-type silicon (100) wafers (polished on both sides) were used as substrates. Octadecyltrichlorosilane (ODTS, $C_n$: 18), dodecyltrichlorosilane (DDTS, $C_n$: 12), and octyltrichlorosilane (OTS, $C_n$: 8) were purchased from Sigma-Aldrich, U.S.A., and Lancaster Synthesis, U.K., and were used as received. Isooctane (99.5%, dry) obtained from Sd-fine Chem., India, was used as a solvent. Millipore water was used to hydrate the aluminum and silicon substrates and for contact angle measurements. Diiodomethane ($CH_2I_2$) used for contact angle measurement was obtained from Lancaster Synthesis, U.K. The aluminum substrates were polished mechanically (sequentially with 1−3 $\mu$m and 0.25 $\mu$m diamond paste) to obtain 12−20 nm rms (root-mean-square) roughness and were then sonicated with acetone for 15 min to remove polishing debris. Polished samples were kept in air for 1 h to allow a natural oxide film to form and then kept in Millipore water for 30 min. Finally, the substrates were dried in a stream of dry nitrogen gas and preserved in a desiccator. Silicon wafers were first immersed in mixture of $H_2SO_4$ and $H_2O_2$ (3:1 v/v) solution for 30 min and then washed four times with Millipore water and dried in a stream of dry nitrogen gas. Before SAM deposition, aluminum and silicon substrates were kept in a UV cleaning chamber for 30 min to burn all carbonaceous contaminants, which may block adsorption sites. Substrates were immersed in freshly prepared additive solutions (1 mM) for 1, 3, and 6 h deposition time for ODTS, DDTS, and OTS, respectively, then taken out, rinsed, and washed with isooctane (twice) to remove excess and physisorbed silane molecules.

**2. FTIR.** All spectra were acquired by infrared reflection absorption spectroscopy (IRRAS) in a Perkin-Elmer GX spectrometer equipped with liquid nitrogen cooled mercury cadmium telluride (MCT) detector. All IR spectra reported here were referenced to a bare aluminum substrate and acquired over 712 scans at 4 $cm^{-1}$ resolution with a p-polarized beam. The sample chamber and detector were purged with dry nitrogen gas before starting the experiments and at regular intervals during the experiment. A heating accessory (Harrick, New York, U.S.A.) was used for taking the spectra at different temperatures with an incident angle of 75° from the surface normal. The spectral analyses were carried out with Spectrum v3.02 software (Perkin-Elmer).

**3. Nanotribometer.** Low-load (25−100 mN range) friction and wear measurement were carried out using a nanotribometer (CSM Instruments, Switzerland), consisting of *X*- and *Y*-axis stepper motors linked to a pin-on-disk module and a *Z*-axis stepper motor linked to the measuring head. A removable cantilever is mounted on the measuring head. The cantilever (normal force constant = 0.1493 ± 0.0001 mN/$\mu$m and tangential force constant = 0.0585 ± 0.0002 mN/$\mu$m) associated with two optical sensors (perpendicular to each other in *X* and *Z* directions) is used for measuring the normal and lateral force deflection. The adjustment of range and the position of optical sensors in relation to the mirrors are carried out using a combination of mechanical and software (Tribox 2.7, CSM Instruments, Switzerland) tuning. In the *Z*-direction, a piezo is used to adjust normal force. The coefficient of friction is determined during sliding by measurement of the deflection in

**TABLE 1: FTIR Vibrational Frequencies of Alkylsilane SAMs Deposited on Aluminum Substrate and Their Corresponding Assignments**[17,38,39,46,47]

| peak position of alkylsilane SAMs | | | |
|---|---|---|---|
| C18 | C12 | C8 | assignment |
| $2960 \pm 1$ | $2964 \pm 3$ | $2965 \pm 4$ | $CH_3$ antisymmetric stretching |
| $2918 \pm 1$ | $2921 \pm 1$ | $2925 \pm 1$ | $CH_2$ antisymmetric stretching |
| $2873 \pm 1$ | $2876 \pm 1$ | diffused | $CH_3$ symmetric stretching |
| $2850 \pm 1$ | $2851 \pm 1$ | $2854 \pm 1$ | $CH_2$ symmetric stretching |
| 1096 | 1102 | 1116 | Si−O−Si antisymmetric stretching |
| 982 | 991 | 995 | Si−O−Si symmetric stretching |
| | 852 | 830 | Si−OH mode |

the elastic arm of the cantilever in both horizontal and vertical planes with two high-precision displacement sensors using the optical signal intensity reflected from mirrors of *X* and *Z* force sensors. A 2-mm-diameter 100 Cr6 steel ball is attached to the end of the cantilever. Before attachment, the steel ball was sonicated with acetone to remove dust particles. The life of additive molecules is reported here in terms of laps ($L_c$), or number of disk revolutions, before the coefficient of friction changes from that of the SAM to that of the bare substrate. All measurements were carried out under ambient conditions (relative humidity 40%, temperature 22 °C).

**4. Contact Angle Measurements.** Measurements of the sessile drop contact angle ($\theta$) were performed with Millipore water and $CH_2I_2$ using a contact angle goniometer (Ramé Hart 100-00, U.S.A.). The reported contact angles were averaged over ten separate measurements. An autopipetting system was used to deliver a fixed volume of liquid (2 $\mu$L). An estimate of the surface free energy was obtained by the method of Owens and Wendt.[41]

**5. AFM Measurements.** AFM experiments were performed using an Explorer AFM (Thermo Microscopes, Santa Barbara, U.S.A.) with $Si_3N_4$ cantilevers (Thermo Microscopes) that have a pyramidal tip with a nominal end radius of 50 nm. A V-shaped cantilever (normal force constant = 0.1 N $m^{-1}$) was used to measure normal and lateral forces. All tips were cleaned in a UV chamber (Bioforce Nanosciences, U.S.A.) for 20 min before use. For frictional force measurement, we considered the difference in lateral force images recorded in the forward and reverse scans, and we report here an average of this difference. The lateral force was recorded using 10 $\mu$m × 10 $\mu$m scan area. For roughness measurements, the scanner was allowed to attain stability before imaging.

## Results and Discussion

**1. Characterization of SAMs as Initially Formed.** The structure of monolayers of alkylsilanes (ODTS, DDTS, OTS) self-assembled on aluminum was characterized by infrared spectroscopy and contact angle measurement. Table 1 assigns the observed peak frequencies to vibrational modes. For the ODTS SAM, modes at 1096 and 982 $cm^{-1}$ due to −Si−O−Si− antisymmetric and symmetric stretches reflect the presence of a siloxane network. DDTS and OTS SAMs also show siloxane peaks but shifted toward higher peak frequency. The presence of the Si−OH mode in DDTS and OTS suggests that, unlike in the case of ODTS, the siloxane network is not complete. To characterize the conformational order of alkylsilane monolayers, we use the methylene stretching modes as a benchmark. The frequencies of the methylene antisymmetric and symmetric stretches are in the ranges 2915−2920 and 2846−2850 $cm^{-1}$, respectively, for alkyl chains in all-trans conformation and shift toward 2928 and 2856 $cm^{-1}$, respectively, when the polymethylene chains are in a liquidlike disordered phase.[35,36] Figure 1 shows the methylene and methyl antisymmetric and symmetric stretches ($d^-$, $d^+$ and $r^-$, $r^+$ respectively) of the alkylsilane SAMs. The peak frequencies of the $d^-$ and $d^+$ modes shift toward lower frequency with increase in chain length. The methylene peak frequencies of ODTS are characteristic of chains in a highly ordered, all-trans conformation; those of OTS of a liquid and those of DDTS are intermediate. Table 2 presents the contact angle data of alkylsilane monolayers. The difference between the contact angles of water on the ODTS and DDTS monolayers is insignificant. A contact angle of 109−110° ($\theta_{water}$) and low surface free energy (23−24 mJ $m^{-2}$) indicates high hydrophobicity for conformationally ordered SAMs. A comparatively low contact angle ($\theta_{water} = 100° \pm 1°$) for OTS reveals a more disordered SAM.

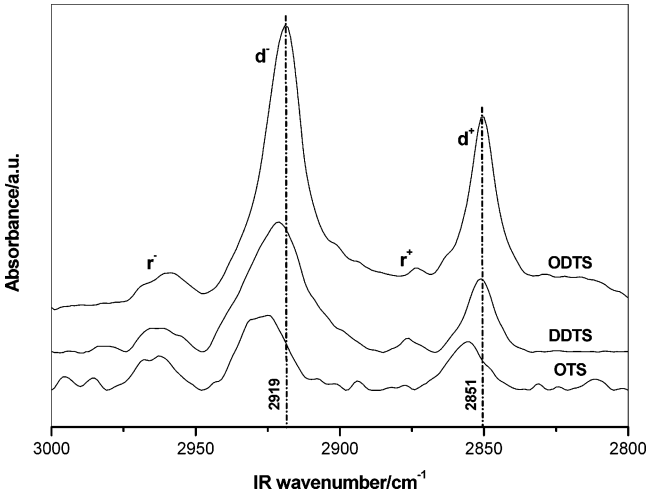


**Figure 1.** Representative FTIR spectra of alkylsilane (ODTS, DDTS, and OTS) monolayers self-assembled on aluminum showing methylene and methyl stretch shifts with chain length.

**TABLE 2: Sessile Drop Contact Angle and Surface Free Energy of Alkylsilane Monolayers Self-Assembled on Aluminum, as a Function of Chain Length**

| monolayer | contact angle, $\theta_{water}$ | surface free energy/mJ.$m^{-2}$ |
|---|---|---|
| ODTS | $110 \pm 1$ | $23 \pm 1$ |
| DDTS | $109 \pm 1$ | $24 \pm 1$ |
| OTS | $100 \pm 1$ | $26 \pm 1$ |

**2. Thermal Behavior of SAMs.** Figure 2a shows the temperature dependence of the peak frequency of the $d^-$ mode for alkylsilane monolayers on Al. For ODTS, the peak frequency increases monotonically from 2918 to 2924 $cm^{-1}$ in the range 24−170 °C and then shows a plateau from 170 to 250 °C. The frequency of the $d^-$ stretch of OTS remains approximately constant at 2925−2926 $cm^{-1}$ up to temperatures of 180 °C. For DDTS, the peak frequency first increases from room temperature up to 80 °C, remains constant at a value of ∼2924 $cm^{-1}$ until 140 °C, and then rises steeply. Figure 2b shows the variation in the integrated intensity in the C−H stretching region ($d^-$ mode) with temperature. Two competing effects control the intensity of the $d^-$ modes: (a) gauche defect generation (increase the intensity) and (b) untilting (decrease the intensity),[17] while thermal desorption decreases the intensity. For both ODTS and DDTS, there is an increase in the integrated intensity that parallels the blue shift in the $d^-$ mode and is therefore ascribed to gauche defect generation. The OTS SAM is already highly disordered at room temperature, and heating does not increase

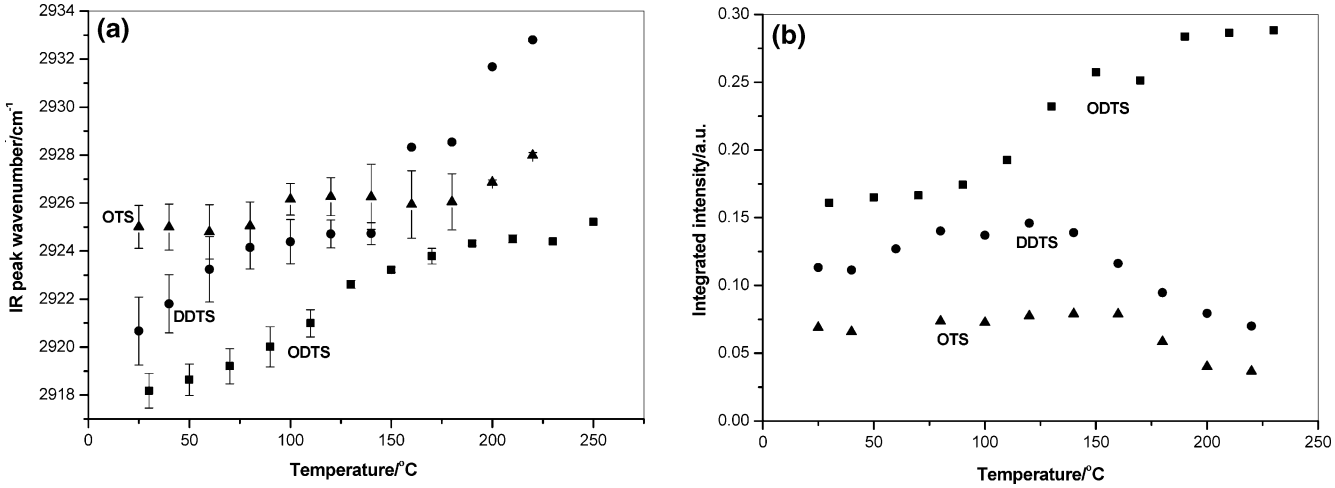


**Figure 2.** (a) Temperature-dependent variations of IR peak wavenumber of methylene antisymmetric stretch for alkylsilane monolayers, ODTS (■), DDTS (●), and OTS (▲), self-assembled on aluminum. The bars show ($\pm\sigma$) standard deviations of experimental points. (b) Temperature-dependent variations of integrated intensity of methylene antisymmetric stretch of alkylsilane monolayers, ODTS (■), DDTS (●), and OTS (▲), self-assembled on aluminum obtained for heating part of thermal cycles.

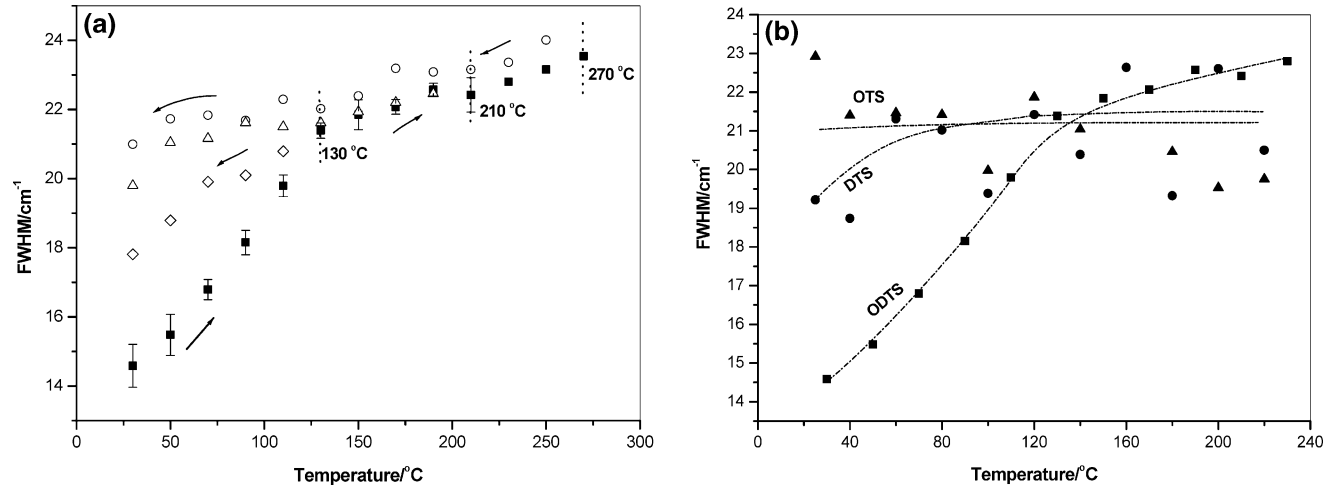


**Figure 3.** (a) Temperature-dependent variations of fwhm of methylene antisymmetric stretch of ODTS monolayer for different thermal cycles. (■) heating to 270 °C, (○) cooling from 270 °C, (△) cooling from 210 °C, and (□) cooling from 130 °C. (b) Temperature-dependent variations of fwhm of methylene antisymmetric stretch of alkylsilane monolayers, ODTS (■), DDTS (●), and OTS (▲), self-assembled on aluminum obtained for heating part of thermal cycles.

**TABLE 3: Residual Integrated Intensity of d$^-$ Mode for Alkylsilane Monolayers at Room Temperature after Heat Treatment**

| monolayer | ODTS | | | DTS | | | OTS | | |
|---|---|---|---|---|---|---|---|---|---|
| heat treatment temperature/°C | 24 | 130 | 210 | 24 | 80 | 140 | 24 | 80 | 140 |
| integrated intensity/a.u. | 0.16 | 0.21 | 0.27 | 0.11 | 0.125 | 0.13 | 0.06 | 0.06 | 0.07 |

the gauche defect population (an effect we term "gauche defect saturation"). From a comparison of Figure 2a and b, we can ascribe the increase in frequency of the d$^-$ mode in DDTS and OTS at high temperatures to desorption of the molecules of the SAM. The residual intensity after heat treatment for the test silanes is given in Table 3. The thermal behavior of ODTS is similar to that of a SAM of octadecanethiol on gold,[39] which has a low population of defects at room temperature and does not show saturation of defects until the desorption temperature. The present data for silanes suggest that defect saturation occurs at 80 °C for DDTS and 170 °C for ODTS, while for OTS, the monolayer is already liquidlike at room temperature.

The bandwidth of the C−H stretch modes is another spectral parameter that is known to correlate with the packing of alkyl chains in monolayer.[37,38] The full width at half-maximum (fwhm) ($\Delta\nu_{1/2}$) of the d$^-$ mode in the crystalline chains of octadecanethiol and *n*-$C_{20}H_{42}$ is 11−13 cm$^{-1}$ at room temperature. For loosely packed chains with a high degree of rotational and translational mobility, $\Delta\nu_{1/2}$ is >18 cm$^{-1}$.[42] Figure 3a shows how $\Delta\nu_{1/2}$ of ODTS varies during heat treatment cycles. At room temperature, $\Delta\nu_{1/2}$ (14 cm$^{-1}$) is close to, but a little higher than, the value for a crystalline alkane.[38] The bandwidth increases steeply with temperature up to a value of $\Delta\nu_{1/2} = 21$ cm$^{-1}$ at 130 °C and more slowly thereafter. The increase in mobility of the chains, indicated by the bandwidth, correlates with the increases in peak frequency and intensity shown in Figure 2. Importantly, the value of $\Delta\nu_{1/2}$ of the d$^-$ mode does not return to its initial value on cooling. The higher the peak temperature of the heating cycle is, the higher the bandwidth at room temperature after cooling. Thus, heat treatment provides a

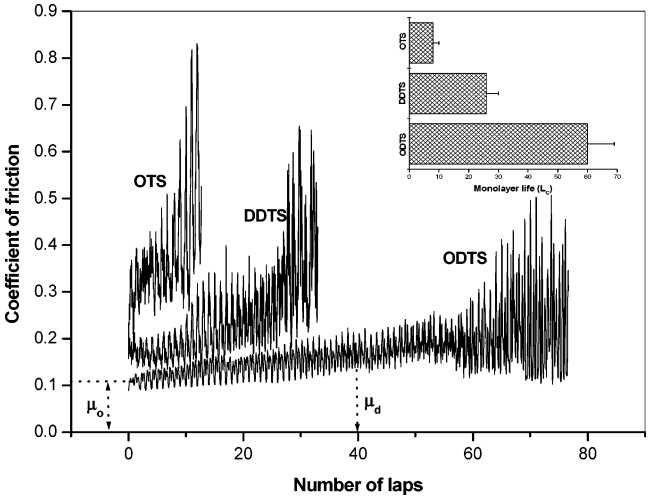


**Figure 4.** Variation in coefficient of friction vs number of laps for alkylsilane (ODTS, DDTS, and OTS) monolayers self-assembled on aluminum (roughness: 12−20 nm, rms). Slid against a 100 Cr6 steel ball of diameter 2 mm and roughness 4 nm rms. Measurements were taken at a normal load of 50 mN with 1 mm/s sliding speed. $\mu_o$: initial coefficient of friction. $\mu_d$: dynamic coefficient of friction. Inset shows the life of monolayers measured as the number of laps (disk revolutions) taken to recover the coefficient of friction (∼0.4) for bare substrate.

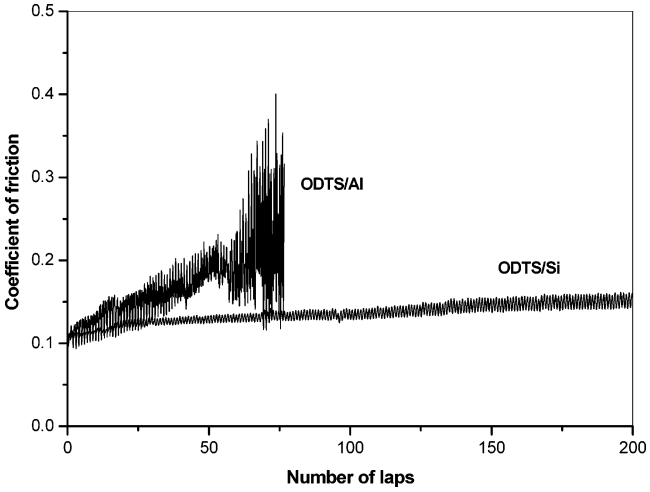


**Figure 5.** The substrate effect: Coefficient of friction ($\mu_d$) vs number of laps of sliding for ODTS SAM deposited on aluminum and silicon. On both substrates, the initial coefficient of friction is the same, but for SAM on aluminum, $\mu_d$ increases rapidly with laps of sliding compared to what is observed for SAM on silicon substrate.

mechanism for introducing disorder into a SAM in a controllable way without changing the identity of the molecule forming the SAM. For completeness, the bandwidth data for the three different alkyl chain lengths is shown in Figure 3b. The trends parallel those observed in Figure 2.

**3. Tribology.** Figure 4 shows typical traces of the coefficient of friction in the nanotribometer as a function of the number of laps for three different alkylsilane SAMs on aluminum. For comparison, Figure 5 shows the frictional characteristics of ODTS on aluminum (rough) and silicon (smooth). We will focus our discussion on three features of these traces: first, the dependence of the initial coefficient of static friction ($\mu_o$) on the structure of the SAM; second, the increase in the dynamic coefficient of friction ($\mu_d$) with the number of laps; third, the critical number of laps ($L_c$) at which large fluctuations in the friction force are recorded and after which the friction coefficient of the substrate ($\mu \approx 0.4$) is recovered; we consider $L_c$ to be the life of the monolayer.

*(i) Initial Coefficient of Friction ($\mu_o$).* In the sliding of a rigid probe on a monolayer, the contact conditions at the commencement of sliding may be different from those during steady-state sliding. The difference may arise from (1) the fact that the contact area is smaller and the penetration greater during sliding than those at the commencement of sliding; only the leading surface of the spherical tip is in contact during sliding; (2) the generation of microscopic debris, and (3) the generation of frictional heat. These effects would tend to degenerate the contact conditions and promote direct probe−substrate contact; this would have the effect of bringing the substrate property into consideration in influencing friction coefficient during sliding. We thus believe that the friction coefficient at the commencement of sliding is perhaps the most faithful representation of the monolayer property, compared with that during any other part of the sliding history. We attempt to establish that $\mu_o$ is genuinely a property of the SAM and not that of the substrate, by comparing $\mu_o$ of the ODTS SAM on the polished aluminum surface (rms roughness = 12−20 nm, Figure 6) and on a silicon (rms roughness = 1−2 nm). The value of $\mu_o = 0.1 \pm 0.01$ is the same on both substrates.

The dependence of $\mu_o$ on chain length and thermal cycling for silane monolayers on Al is displayed in Figure 7. The initial coefficient of friction (always measured at room temperature) increases with decreasing chain length and with increasing heat treatment temperatures. Comparison with the FTIR data in Figures 2 and 3 show that $\mu_o$ is correlated with the initial state of disorder of the monolayer, as shown by the peak frequency and bandwidth of the methylene stretching modes. This correlation is shown quantitatively in Figure 8, where we have plotted $\mu_o$ against $\Delta\nu_{1/2}$ for SAMs with different chain lengths and heat treatment temperatures. There is a surprisingly good linear relationship between the two parameters. This correlation suggests that the molecular degrees of freedom that give rise to the broadening of the bandwidth of the chain modes also provide avenues for efficient dissipation of energy and hence to high friction. A similar conclusion has previously been drawn from LFM results.[22]

All the SAMs tested here (ODTS, DDTS, and OTS, both non-heat-treated and heat-treated) at the commencement of sliding obey Amonton's law, i.e., the friction coefficient is independent of load. Further, the initial friction force for all test SAMs tends to zero at zero load. These observations suggest that adhesion between the SAM and the substrate and deformation of the SAM under load play a negligible role in determining friction, at least in the initial stage of sliding. These results obtained using nanotribometer are somewhat different from those obtained using the LFM[11] for alkylsilane monolayers. The LFM results obtained in a mean pressure range of 0−600 MPa, compared to the present pressure range of 50−100 MPa, show nonzero friction force at zero normal load and a variable coefficient of friction with normal load, although the order of friction coefficient recorded is the same as that observed here.

*(ii) Dynamic Coefficient of Friction ($\mu_d$).* Figure 9 plots the dynamic coefficient of friction ($\mu_d$) as a function of load after the SAM has been slid for a finite number of laps. As in the case of $\mu_0$, the shorter chain length gives higher friction.[7,22] However, in the dynamic case (compare ODTS/Al at 20 laps with DDTS/Al at 15 laps), the normal load influences the friction strongly. Two different explanations for the dependence of $\mu_d$ on load have been proposed in the literature. Salmeron,[32] on the basis of his LFM studies, assigns the variation in $\mu_d$ to load-

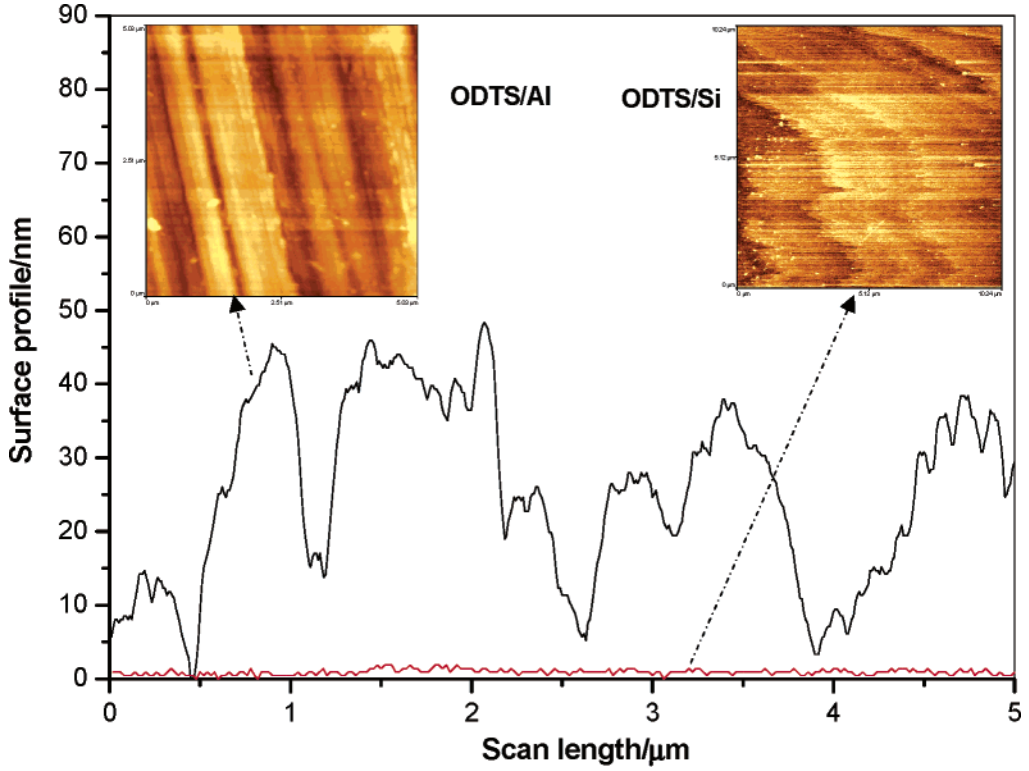


**Figure 6.** Surface profile of ODTS monolayer on aluminum and silicon substrate with their topography images, taken by AFM.

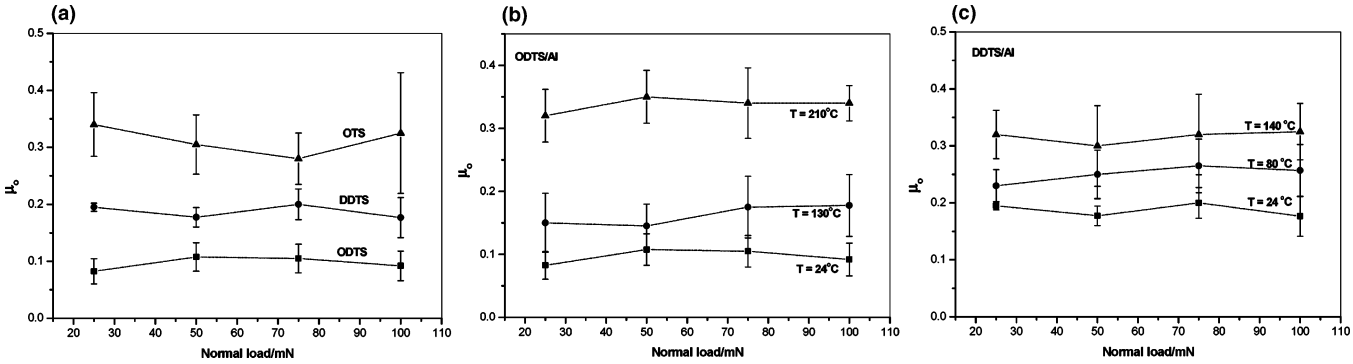


**Figure 7.** Initial coefficient of friction, $\mu_o$ vs normal load (a) for ODTS (■), DDTS (●), and OTS (▲) monolayers assembled on aluminum. $\mu_o$ is more or less independent of load, although it increases with reducing chain length. (b) Change in $\mu_o$ with heat treatment peak temperatures of 24 °C (■), 130 °C (●), and 210 °C (▲) for ODTS. (c) Change in $\mu_o$ with heat treatment peak temperatures of 24 °C (■), 80 °C (●), and 140 °C (▲) for DDTS. $\mu_o$ increases with heat treatment temperature for both systems. OTS monolayer exhibits substrate coefficient of friction after heat treatment; the data are not presented here.

induced changes in molecular conformation, while Yoshizawa et al.[3] have suggested on the basis of their SFA studies that thermally induced change in crystallinity is a reason for changes in friction. A reversible conformational change under load in our experiments is inconsistent with two pieces of evidence. First, $\mu_0$ is not affected by load. Second, $\mu_d$ increases with number of laps. A thermal origin to the increase in $\mu_d$ with time is also unlikely. If thermal disordering were important, then we would see a larger increase in $\mu_d$ in ODTS on silicon than on aluminum, since the former substrate has a lower thermal conductivity and higher Young's modulus (and hence, the sliding energy is dissipated in a smaller area). We observe the reverse (Figure 5). Furthermore, an order of magnitude estimate of the contact temperature based on the frictional energy dissipated and the thermal conductivity of aluminum shows that the rise in contact temperature above ambient is negligible (the monolayer itself will thermally equilibrate very rapidly with the substrate). Even local heating of asperity contacts is unimportant at the slow sliding rates employed in our experiments (1 mm $s^{-1}$).

To explain the differences observed between silicon and aluminum substrates, we consider the role played by plasticity. Figure 10 shows the roughness profile of the SAM as deposited on aluminum and after 20 and 40 laps. The high-frequency surface oscillations seen on the as-deposited SAM disappear by 20 laps to be replaced by large low-frequency undulations. After 40 laps, the low-frequency undulations remain, but some high-frequency oscillations reappear on the surface, yielding a slightly higher rms amplitude (Table 4). The mean pressure, $p_m$, on a 25-$\mu$m-wide track is ~0.1 GPa. On a rough surface, however, initial contact is only made between asperities, where the local pressure is very likely to exceed the yield stress of aluminum (1 GPa, load = 3mN, Berkovich indentor). Consequently, the aluminum may undergo plastic deformation,[43]

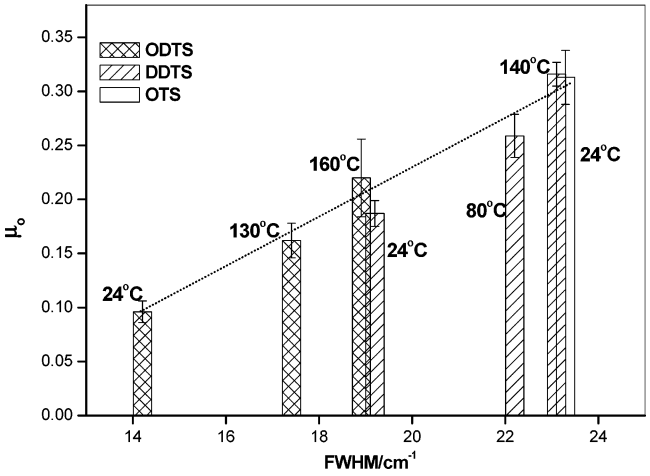


**Figure 8.** Plot of fwhm vs initial coefficient of friction ($\mu_o$) for alkylsilane (ODTS, DDTS, and OTS) monolayers at different heat treatment temperatures. Values of fwhm were obtained from methylene antisymmetric ($d^-$) stretch mode. Here, $\mu_o$ shows a rough linear correlation with fwhm.

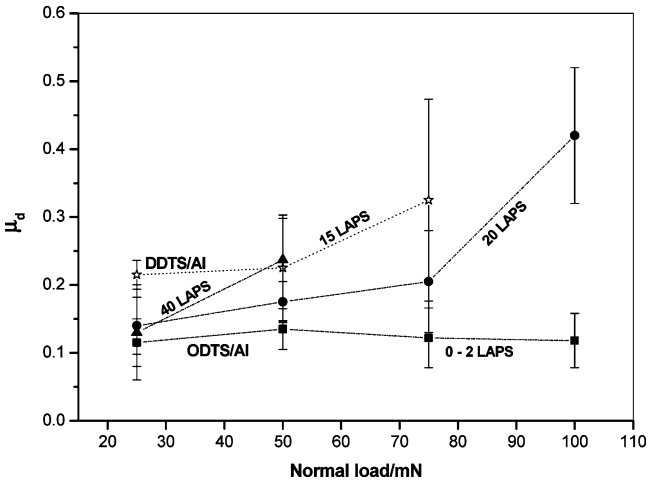


**Figure 9.** Variation of dynamic coefficient of friction, $\mu_d$, vs normal load as a function of number of laps slid: (■) 0−2 laps, (●) 20 laps, and (▲) 40 laps for ODTS and (☆) 15 laps for DDTS SAM. The figure demonstrates that, when a SAM is anchored on rough aluminum, and has been slid for a finite number of laps, the coefficient of friction increases with normal load. This is in contrast to the insensitivity of the coefficient of friction to normal load observed at the commencement of sliding.

leading to gross morphological changes in the surface. Asperities (indicated by the high-frequency oscillations in Figure 10) initially present on the virgin aluminum substrate appear to be removed completely by plastic deformation after 20 laps of sliding. Indentation by plastic flow also reshapes the subsurface region, eliminating the polishing scratches on the virgin substrate and creating low-frequency undulations.

It is worth noting that, after 40 laps compressed in a conformal contact and under plastic flow, the monolayer is still at least partially intact: the value of $\mu_d = 0.15$ is significantly less than that of the bare substrate ($\mu_d \approx 0.4$). This ability of SAMs to maintain lubricity when the substrate is deformed has also been demonstrated by Nie et al.[44] for octadecylphosphonic acid on mica being scratched by a diamond stylus. Although the substrate is grossly plastic under load, the cross-sectional line length changes very little (less than 1%) with sliding (Table 4). Consequently, the average density of the SAM is not greatly affected by plastic flow. It might appear that, although plastic

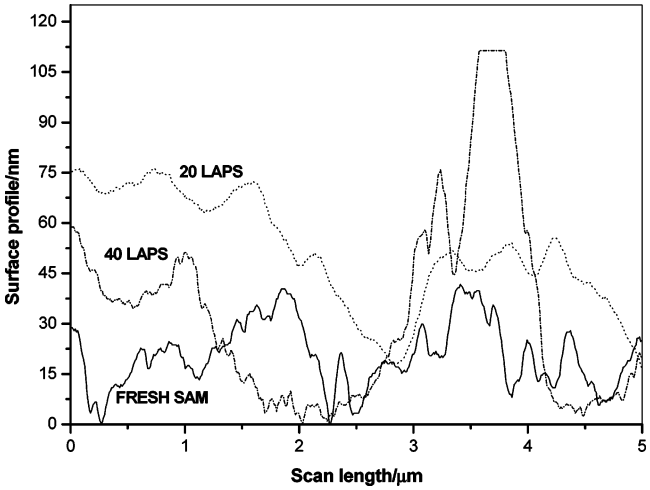


**Figure 10.** Surface profile of ODTS monolayer on aluminum after different number of laps sliding, taken using AFM.

**TABLE 4: Change in Roughness Profile and Cross-Sectional Line Width Ratio of ODTS Modified Aluminum Surface under the Track with Different Number of Laps**

| SAM | roughness (rms) under track area (nm) | cross-sectional line length ratio, $X^*$ (nm/nm) |
|---|---|---|
| FRESH OTS | 12 ± 1 | 1.008 |
| 5 LAPS | 15 ± 2 | 1.002 |
| 20 LAPS | 29 ± 2 | 1.004 |
| 40 LAPS | 30 ± 1 | 1.006 |
| 50 LAPS | 36 ± 2 | 1.006 |


$$X = \frac{\Sigma t_i}{\Sigma l_i}$$

deformation is occurring, neither heat generation nor a global reduction in packing density can account for the increase in dynamic friction that we observe for SAMs on aluminum (Figure 5).

Additional insight into the tribological changes taking place under sliding can be gained from lateral force imaging of the aluminum surface within the contact region from the nanotribometer (Figure 11). After 20 laps, we observe high-friction grooves, which run in the sliding direction, while the total contact width is 25 $\mu$m. We thus have an instantaneous apparent contact spot of 25 $\mu$m diameter. The width of most of these grooves (Figure 11b) varies between 20 and 150 nm (such high-friction grooves are not seen on the SAM on silicon even after 500 laps of sliding). A plausible origin of these grooves is plastic ploughing by asperities on the steel ball attached to the cantilever of the nanotribometer. By taking the hardness of the Al surface to be 1 GPa and assuming the instantaneous contact to consist of parallel grooves of 100 nm width and 10 $\mu$m length (an average in a 25-$\mu$m-diameter circular contact spot), then if the applied load (50 mN) is equally shared by these grooves there would be about 50 such permanent (plastically deformed) grooves on the surface, which should roughly conform to the asperity shape. A count of grooves in the LFM images gives about this number. The average strain in a fully plastic groove is $\sim a/R$,[43] where $a$ is the half-width of the groove and $R$ is the average radius of the asperity (on the steel ball as obtained from profilometric measurement). For $a = 50$ nm and $R = 330$ nm

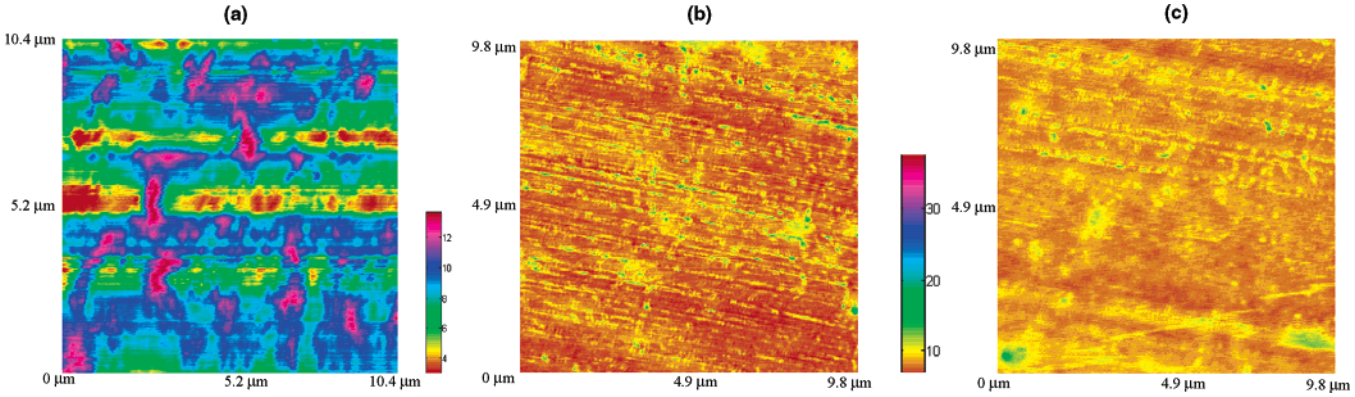


**Figure 11.** Friction images of ODTS monolayer taken in the LFM mode of AFM before sliding in the nanotribometer. (a) Fresh ODTS SAM on aluminum. After sliding in the nanotribometer with normal load of 50 mN and sliding speed of 1 mm/s. (b) ODTS SAM on aluminum after 20 laps, showing, in general, higher friction than in (a) and high-friction grooves of 20−150 nm width in the sliding direction. (c) ODTS SAM after 40 laps showing an increase in the width of high-friction grooves compared to what is observed after 20 laps.

(average tip radius), the average strain induced is about 14%.[43] We may therefore expect to reduce the spatial density of the molecule in the SAM locally by about 14%. If we now take into account that a reduction in packing density increases[31,45] friction, we could expect lean areas on the surface to generate high friction. Figure 11 suggests that there is a progressive degeneration of the surface where the areas of local high friction or low packing density expand with sliding distance (compare the LFM images after 20 laps and 40 laps).

Our results therefore indicate that localized plastic deformation occurs on the substrate surface due to high pressures transmitted by the probe asperities of nanometric dimensions. The affected zone stretches permanently, normal to the sliding direction, in creating a groove. The substrate is rough at a scale which is macroscopic in comparison to the microscopic grooves; the local micro plasticity therefore does not change the cross-sectional line length (Figure 10). We believe that the monolayer being slid conforms to the stretched plastic grooves, giving rise to a reduction in local line density of monolayer packing. If the increase in friction with sliding is indeed related to this phenomenon, it implies that the self-assembled monolayer persists under sliding conditions, demonstrating mobility as well as significant load support.

For ODTS on silicon, the increase in $\mu_d$ with the number of laps is much lower than for aluminum (Figure 5), and there is no evidence from AFM of an increase in roughness or from LFM of high-friction grooves. A simple explanation for the difference in behavior is that silicon is much harder than aluminum (hardness = 12 GPa compared to 1 GPa for aluminum) and that it deforms elastically rather plastically in contact with the steel ball of the nanotribometer.

*(iii) Monolayer Life ($L_c$).* For each of the alkylsilane monolayers on aluminum, $\mu_d$ increases with the number of laps but remains approximately constant over a single lap. (The data in Figures 5 and 6 show a superimposed oscillation with the period of rotation that arises from macroscopic unevenness in the aluminum disk.) After a critical number of laps, $L_c$, the frictional force becomes highly irregular and the mean coefficient of friction approaches that of the bare aluminum substrate. We associate the breakdown in lubrication with the localized removal of sufficient monolayer material that metal−metal or metal−oxide contacts form. The wear debris arising from these strongly adhesive contacts then leads to rapid breakdown of the monolayer on other areas of the surface. The lifetime of the monolayer increases with increasing chain length and decreases with heat treatment temperature as shown in Figure 12. ODTS

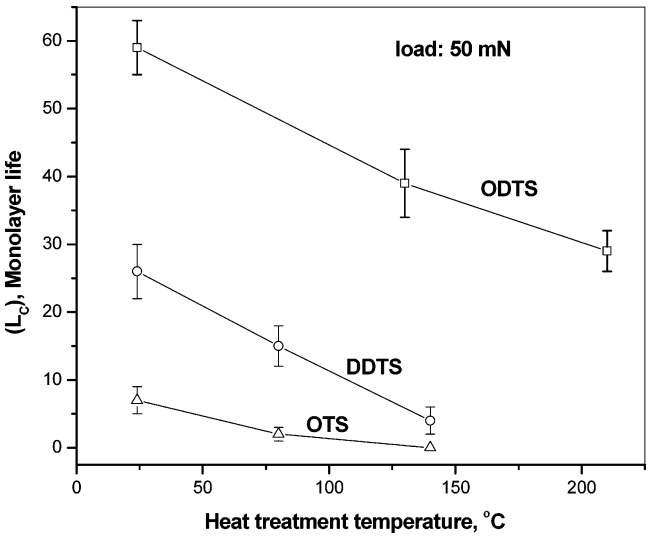


**Figure 12.** Variation of monolayer life with chain length and heat treatment temperature, measured by nanotribometer at 50 mN load for ODTS (□), DDTS (○), and OTS (△).

on silicon shows similar catastrophic breakdown of lubrication, but only after 3000 laps. In contrast to the monolayers on aluminum, there is no significant wear of the silicon substrate prior to $L_c$, at which point, rapid wear occurs. This observation is consistent with the idea that it is the generation of the initial wear debris that lead to the catastrophic breakdown in lubrication. We ascribe the large difference in the values of $L_c$ for ODTS on aluminum and silicon to plastic deformation of the aluminum surface that leads to a reduction in the local density of the lubricating molecules and an enhanced probability of metal−substrate contacts.

Increasing the normal load increases the value of $\mu_d$ after a finite number of laps (Figure 9) and commensurately reduces the number of laps to failure of the lubricating film, $L_c$. This behavior is consistent with the mechanism of plastic deformation proposed above. If this description of the process is correct, we should expect the life of a SAM to be influenced by (a) the initial packing density of the SAM, the substrate roughness remaining constant, and (b) the normal load, which would tend to accentuate the deformation and wear of the substrate. Recognizing that the fwhm obtained from our FTIR studies of freshly prepared SAMs is an indicator of packing density, we plot in Figure 13 a "life map" of alkylsilane SAMs deposited on an engineering aluminum surface. The surface drawn through

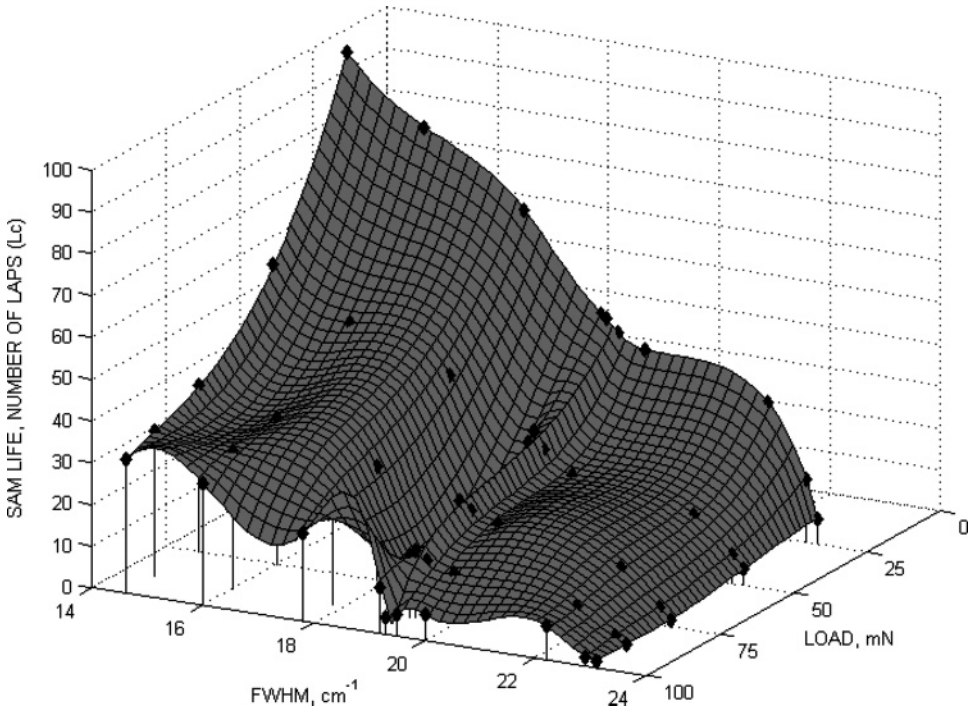


**Figure 13.** Life map of alkylsilane monolayers deposited on aluminum surface as a function of a priori fwhm of SAM and normal load. The number of laps of sliding done to recover the substrate coefficient of friction (~0.4) is taken as the life of a SAM. Experimental data of SAM life of ODTS, DDTS, and OTS molecules heat-treated to different (test) peak temperatures are incorporated in the figure.

experimental points shows how the life of the SAM decreases with a reduction in packing density and increasing normal load. The trend observed in monolayer life due to change in chain length and heat treatment temperature as shown in Figure 13 should only be taken as a broad indicator, as no attempt was made to vary the chain length continuously and the heat treatment temperatures were also chosen arbitrarily.

## Conclusion

In this paper, we have explored the tribology of boundary lubricants formed by adsorption of monolayers of alkylsilanes on a polished but microscopically rough aluminum surface. The experiments were performed in a nanotribometer at a mean contact pressure of 0.1 GPa. By taking a typical dimension of an asperity to be 100 nm and the sliding rate of 1 mm $s^{-1}$, the boundary lubricants are in mechanical contact with the slider for about 0.1 ms in any particular event. On this time scale, heat generated within the asperity diffuses rapidly into the bulk aluminum substrate, so transient thermal effects are negligible. The friction coefficient, $\mu_0$, at the commencement of sliding was independent of normal load, suggesting that reversible conformational changes under load, of the type observed in LFM studies, are unimportant in the nanotribometer. We do find, however, that $\mu_0$ found is correlated to the initial conformational order of the SAM, which was experimentally varied by changing the chain length and heat treatment of the monolayers. In this respect, the results agree with those generated by others by lateral force microscopy.

While the structures and initial coefficients of friction of ODTS monolayers on aluminum and silicon are similar, the performances of these monolayers under prolonged sliding are very different. In both cases, $\mu_d$ increases with number of laps but at a rate that is 2 orders of magnitude faster on aluminum than on silicon, despite the higher mean contact pressures in the latter case. The poorer performance of monolayers on aluminum is ascribed to the plasticity of the substrate. Plastic deformation of the aluminum results in a local reduction in the density of the protective monolayer, which increases dissipation and leads to an increased probability of lubricant breakdown and wear of the substrate. Empirically, we have observed that the greater the initial disorder in the monolayer is, the shorter the life of the lubricating film. Since plastic deformation is load dependent, it is not surprising that $\mu_d$ is dependent on load, so Amonton's Law is no longer obeyed.

In contrast to aluminum, the silicon substrate does not deform plastically under the conditions of the nanotribometer. Friction still increases with the number of laps, but in the absence of substrate deformation, the rate of increase is much slower than for aluminum. The molecular origin of the increased friction in SAMs on silicon was not explored in this study. Nevertheless, it is clear that the qualitative difference in modes of dissipation made by the roughness and mechanical properties of the substrate brings about a substantial difference in the friction and life of the self-assembled molecular layer.

The present study is of engineering relevance, as it puts a limit on the roughness and compliance of the substrate on which a lubricating monolayer is assembled for cases, such as microelectromechanical systems or storage hard disks, where the assembly is done once in the lifetime of a machine. We believe that it also has wider relevance in macrotribological applications such as bearings and engines, where additive molecules dispersed in base oil assemble onto a substrate and provide protection and reduced power dissipation in tribological situations. If the nature of the slider or the substrate is detrimental to the life of the SAM and/or promotes large variations in friction force in a cycle generating severe stick slip, changes in design of components may be necessary to ensure optimum performance.

**Acknowledgment.** The authors are grateful to Centre for High Technology (CHT), Ministry of Petroleum, Govt of India, and General Motors (R & D), Warren, U.S.A., for the financial grant which has made this work possible. They also acknowl-

edge the help of Mrs. S. Savitha, Ms. N. Prathima, and Mr. H. S. Shamasunder in carrying out this work.

## References and Notes

(1) Ulman, A. *An introduction to ultrathin organic films from Langmuir−Blodgett to self-assembly*; Academic Press: New York, 1991.
(2) Israelachvili, J. N. *Intermolecular and surface forces*, 2nd ed.; Academic Press: London, 1997.
(3) Yoshizawa, H.; Chen, Y. L.; Israelachvili, J. *J. Phys. Chem.* **1993**, *97*, 4128.
(4) Zhang, Q.; Archer, L. A. *J. Phys. Chem. B* **2003**, *107*, 13123.
(5) Bhushan, B.; Israelachvili, J. N.; Landman, U. *Nature (London)* **1995**, *374*, 607.
(6) McDermott, M. T.; Green, J. D.; Porter, M. D. *Langmuir* **1997**, *13*, 2504.
(7) Lio, A.; Charych, D. H.; Salmeron, M. *J. Phys. Chem. B* **1997**, *101*, 3800.
(8) Liu, H.; Ahmed, U. I.; Scherge, M. *Thin Solid Films* **2001**, *381*, 135.
(9) Devaprakasam, D.; Khatri, O. P.; Shankar, N.; Biswas, S. K. *Tribol. Int.* In press.
(10) Carpick, R. W.; Salmeron, M. *Chem. Rev.* **1997**, *97*, 1163.
(11) Barrena, E.; Kopta, S.; Ogletree, D. F.; Charych, D. H.; Salmeron, M. *Phys. Rev. Lett.* **1999**, *82*, 2880.
(12) Yang, X.; Perry, S. S. *Langmuir* **2003**, *19*, 6135.
(13) Piao, H.; Mclntyre, N. S. *Surf. Interface Anal.* **2001**, *31*, 874.
(14) Hoffmann, H.; Mayer, U.; Krischanitz, A. *Langmuir* **1995**, *11*, 1304.
(15) Kojio, K.; Takahara, A.; Kajiyama, T. *Langmuir* **2000**, *16*, 9314.
(16) Parikh, A. N.; Allara, D. L.; Azouz, I. B.; Rondelez, F. *J. Phys. Chem.* **1994**, *98*, 7577.
(17) Khatri, O. P.; Biswas, S. K. *Surf. Sci.* **2004**, *572*, 228.
(18) Wasserman, S. R.; Tao, Y. T.; Whitesides, G. M. *Langmuir* **1989**, *5*, 1074.
(19) Xiao, X. D.; Liu, G.; Charych, D. H.; Salmeron, M. *Langmuir* **1995**, *11*, 1600.
(20) Bierbaum, K.; Grunze, M.; Baski, A. A.; Chi, L. F.; Schrepp. W.; Fuchs, H. *Langmuir* **1995**, *11*, 2143.
(21) Wang, Y.; Lieberman, M. *Langmuir* **2003**, *19*, 1159.
(22) Xiao, X.; Hu, J.; Charych, D. H.; Salmeron, M. *Langmuir* **1996**, *12*, 235.
(23) Brzoska, J. B.; Shahidzadeh, N.; Rondelez, F. *Nature (London)* **1992**, *360*, 719.
(24) Foisner, J.; Glaser, A.; Kattner, J.; Hoffmann, H.; Friedbacher, G. *Langmuir* **2003**, *19*, 3741.
(25) Angst, D. L.; Simmons, G. W. *Langmuir* **1991**, *7*, 2236.
(26) Tripp, C. P.; Hair, M. L. *Langmuir* **1992**, *8*, 1120.
(27) Porter, M. D.; Bright, T. B.; Allara, D. L.; Chidsey, C. E. D. *J. Am. Chem. Soc.* **1987**, *109*, 3559.
(28) Granier, M.; Lanneau, G. F.; Moineau, J.; Girard, P.; Ramonda, M. *Langmuir* **2003**, *19*, 2691.
(29) Brewer, N. J.; Beake, B. D.; Leggett, G. J. *Langmuir* **2001**, *17*, 1970.
(30) Tutein, A. B.; Stuart, S. J.; Harrison, J. A. *Langmuir* **2000**, *16*, 291.
(31) Mikulski, P. T.; Harrison, J. A. *J. Am. Chem. Soc.* **2001**, *123*, 6873.
(32) Salmeron, M. *Tribol. Lett.* **2001**, *10*, 69.
(33) Barrena, E.; Ocal, C.; Salmeron, M. *J. Chem. Phys.* **2000**, *113*, 2413.
(34) Cha, K.-H.; Kim, D.-E. *Wear* **2001**, *251*, 1169.
(35) Snyder, R. G.; Strauss, H. L.; Elliger, C. A. *J. Phys. Chem.* **1982**, *86*, 5145.
(36) Macphail, R. A.; Strauss, H. L.; Snyder, R. G.; Elliger, C. A. *J. Phys. Chem.* **1984**, *88*, 334.
(37) Cho, Y.; Kobayashi, M.; Tadokoro, H. *J. Chem. Phys.* **1986**, *84*, 4636.
(38) Wood, K. A.; Snyder, R. G.; Strauss, H. L. *J. Chem. Phys.* **1989**, *91*, 5255.
(39) Prathima, N.; Harini, M.; Rai, N.; Chadrashekara, R. H.; Ayappa, K. G.; Sampath, S.; Biswas, S. K. *Langmuir* **2005**, *21*, 2364.
(40) Devaprakasam, D.; Sampath, S.; Biswas, S. K. *Langmuir* **2004**, 20, 1329.
(41) Owens, D. K.; Wendt, R. C. *J. Appl. Polym. Sci.* **1969**, *13*, 1741.
(42) Evans, S. D.; Berarducci, K. E. G.; Urankar, E.; Gerenser, L. J.; Ulman, A.; Snyder, R. G. *Langmuir* **1991**, *7*, 2700.
(43) Johnson, K. L. *Contact Mechanics*; Cambridge University Press: New York, 2001.
(44) Nie, H. Y.; Miller, D. J.; Francis, J. T.; Walzak, M. J.; McIntyre, N. S. *Langmuir* **2005**, *21*, 2773.
(45) Duwez, A. S.; Jonas, U.; Klein, H. *ChemPhysChem* **2003**, *4*, 1107.
(46) Bensebaa, F.; Ellis, T. H.; Badia, A.; Lennox, R. B. *Langmuir* **1998**, *14*, 2361.
(47) Wang, R.; Baran, G.; Wunder, S. L. *Langmuir* **2000**, *16*, 6298.